SUPPLEMENTARY INFORMATION FOR

Optofluidic Microengine in A Dynamic Flow Environment via Self-Induced Back-Action

Yuzhi Shi[1], Tongtong Zhu[2], Kim Truc Nguyen[1], Yi Zhang[3], Sha Xiong[4], Peng Huat Yap[5], Wee Ser[1], Shubo Wang[6], Cheng-Wei Qiu[7], C. T. Chan[8*], and Ai Qun Liu[1*]

[1] *School of Electrical and Electronic Engineering, Nanyang Technological University, Singapore 639798*

[2] *School of Optoelectronic Engineering and Instrumentation Science, Dalian University of Technology, Dalian 116024, China*

[3] *School of Mechanical and Aerospace Engineering, Nanyang Technological University, Singapore 639798*

[4] *School of Automation, Central South University, Changsha 410083, China*

[5] *Lee Kong Chian School of Medicine, Nanyang Technological University, Singapore 308232*

[6] *Department of Physics, City University of Hong Kong, Tat Chee Avenue, Kowloon, Hong Kong SAR, China*

[7] *Department of Electrical and Computer Engineering, National University of Singapore, Singapore 117583*

[8] *Department of Physics, The Hong Kong University of Science and Technology, Clear Water Bay, Hong Kong, China*

**Corresponding Authors: C. T. Chan (phchan@ust.hk); Ai Qun Liu (eaqliu@ntu.eud.sg)*

1. Illustration of the SIBA effect on the potential well

The illustration of the Self-induced back-action effect on the potential well is shown in Figure S1. The particle initially cannot hop from the primary hotspot to the secondary hotspot because the potential well of the primary hotspot is deep as calculated by the perturbative theory. Because the interaction of light and particle, the potential well is reshaped based on the rigorous Minkowski stress tensor. The potential well of the primary hotspot is flattened to facilitate the hopping of particle to the secondary hotspot.

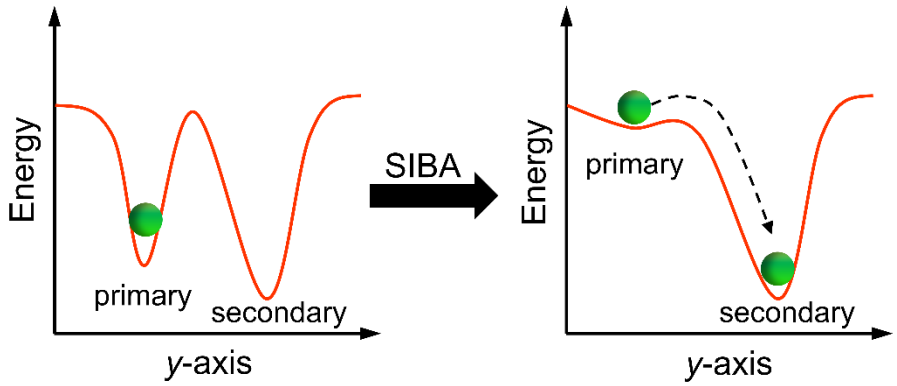

Figure S1. Illustration of the SIBA effect on the shaping of potential well.

2. Generation of asymmetric interference patterns

To generate the asymmetric light interference patterns, we propose two methods. One is the shift of axis of optical fiber as shown in Figure S2a. The other is the tilting of optical fiber as shown in Figure S2b. Because the upper hotspot is very weak and relatively far away from the main hotspot on the left in Figure S2a, there is a higher chance for the particle to hop from the main hotspot to the lower one on the right, resulting in a clockwise cyclic locomotion by the coordinated manoeuvre of the optical and drag forces. The light rays from the optical fiber undergo the constructive and destructive interferences after the microlens to generate the inference patterns in the three schemes in Figure S2. In practice, shifting the

fiber by a short distance (e.g., 1-2 μm) is more difficult than tilting the fiber with a small angle because of the fabrication tolerance in the soft lithography.

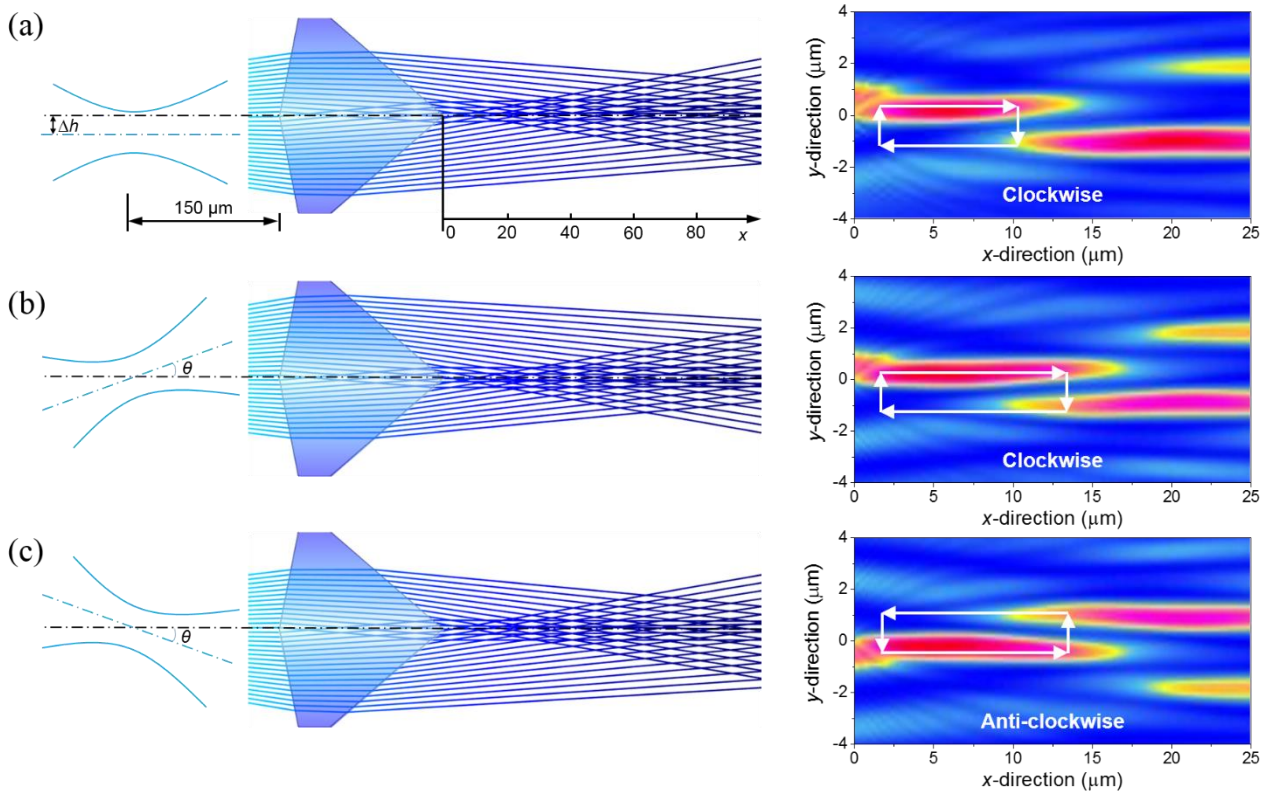

Figure S2. Schemes for the generation of discrete interference patterns. (a) Shifting the axis of Gaussian beam to a Δ*h* in the *y*-direction for the generation of an asymmetric light pattern. Δ*h* used in the simulation is 2 μm. The beam waist of the beam is placed 150 μm away from the microlens in the *y*-direction. (b) & (c) Tilting of the Gaussian beam to an angle θ is used to generate an asymmetric light pattern. θ used in the simulation is 1°. (b) When the angle θ is positive, particle will follow a cycle in clockwise. (c) While, particle will follow a cycle in anti-clockwise if θ is negative.

3. Simulation of light field and optical forces.

We compare the integration of Minkowski stress tensor over a cube and a sphere surface as shown in Figures S3-S5. Both methods show good agreement with each other. We choose the integration over a cube which is 15 nm away from the surface of the particle for faster computing and easy operation.

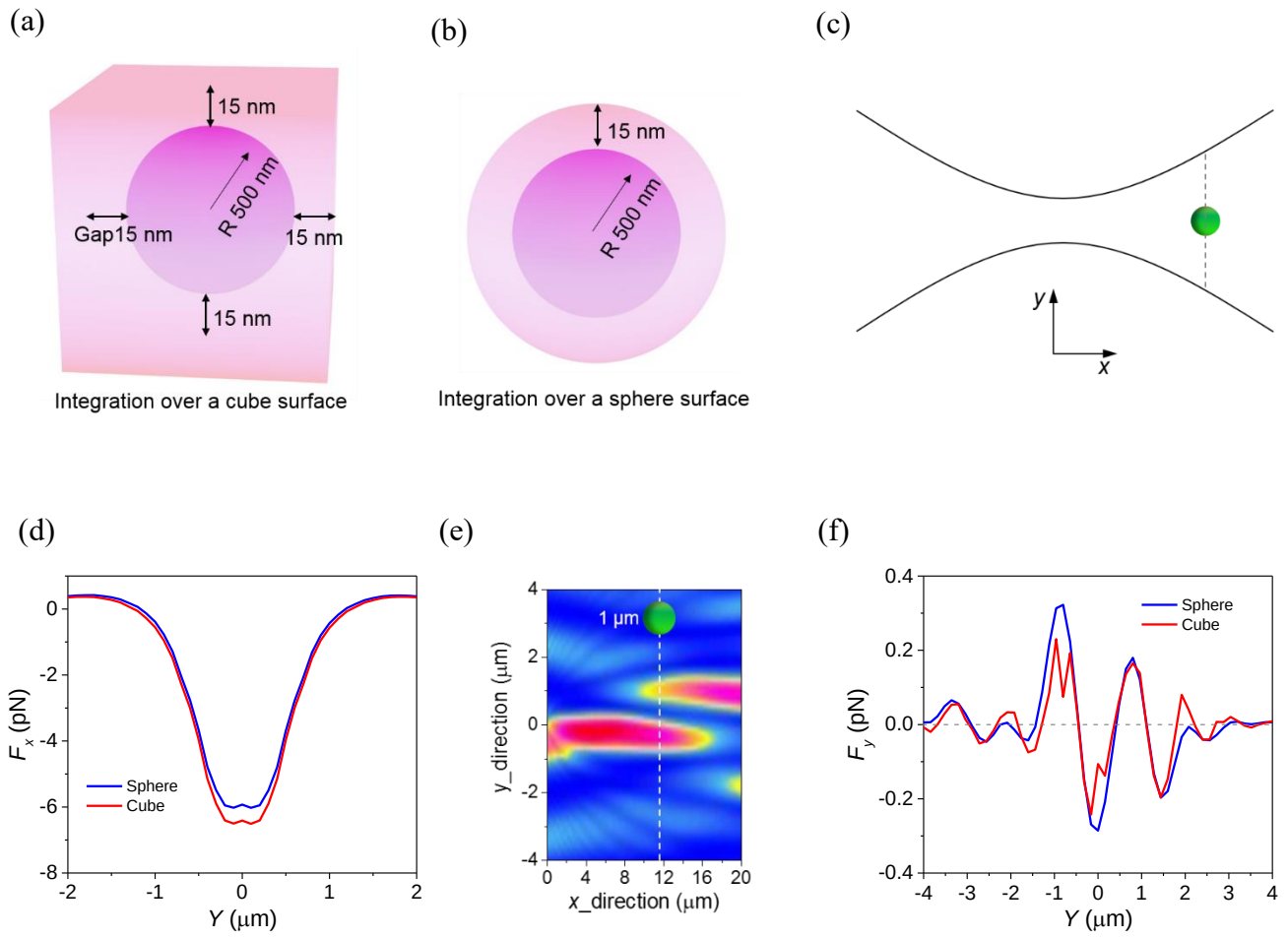

Figure S3. Comparison of integration over the cube and sphere surfaces in water using Minkowski stress tensor. Illustration of the integration over the (a) cube and (b) sphere surface. The radius of the particle is 500 nm. The radii of the cube and the sphere are both 515 nm. The refractive indices of the particle and water are 1.38 and 1.33, respectively. (c) & (d) Comparison of the optical forces in a Gaussian beam. The calculation is along a line with 1 μm away from the beam waist. The numerical aperture of the Gaussian beam is 0.28. (e) & (f) Comparison of the optical forces in the asymmetric light pattern. The simulation over two surfaces are performed in commercial software Lumerical and Matlab. The simulation results with two surface integration show good match with each other.

Since the two-dimensional force field is a non-conservative field with a non-conservative force F_{drag}, we calculate the total force by considering the particle is still in each position to illustrate the energy

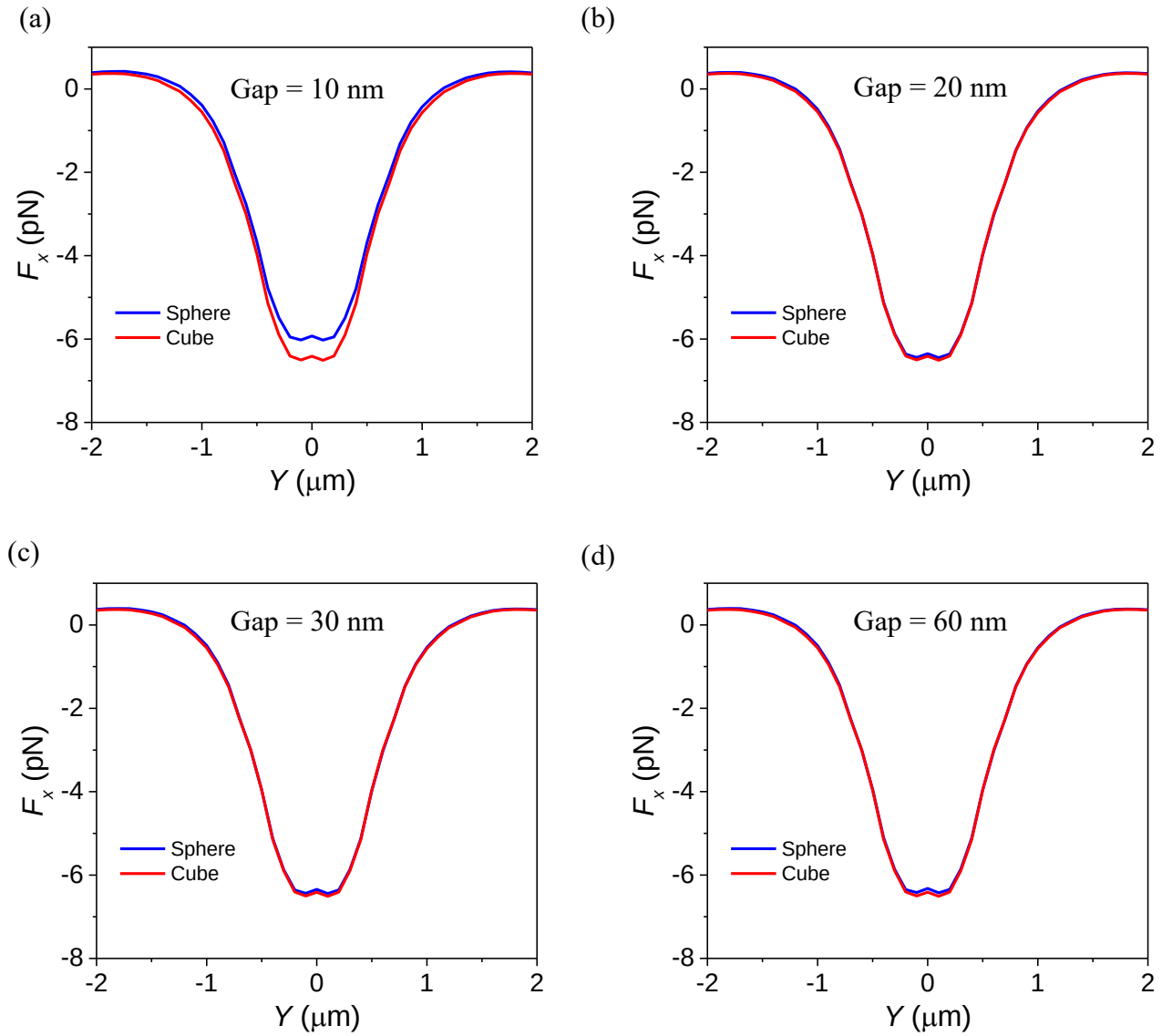

Figure S4. Comparison of the optical force in the *x*-direction in a Gaussian beam by changing the gaps. Calculated forces in the *x*-direction when the gaps between the integration surface and the particle are (a) 10 nm; (b) 20 nm; (c) 30 nm and (d) 60 nm. The maximum mesh in the simulation zone is 10 nm. Two methods match very well when the gaps are 20 nm and 30 nm.

change by the optical and drag forces. Therefore, in each point, the total force can be defined as $F(y, x) = F_{\text{opt}}(y, x) + F_{\text{drag}} = F_{\text{opt}}(y, x) + 6\pi\eta a v$, where η and v are the viscosity and the velocity of the flow, respectively. It is noted that this definition of potential energy may not be suitable for every two-dimensional force field. The method here can illustrate the energy transfer well because that the particle

moves along a rectangle trajectory and the force in the y-direction is mainly contributed by the conservative optical gradient force.

The optical extinction force on a dielectric particle predicted by the Rayleigh theory can be expressed as

$$F_{ext} = F_{sca} = \frac{128\pi^5 R^6 n_m I}{3\lambda^4 c}\left(\frac{m^2-1}{m^2+2}\right)^2 \quad \text{(S1)}$$

with $m = n_p / n_m$,

where R is the radius of the particle, n_{m} is the refractive index of the medium, λ is the wavelength of light, I is the light intensity, c is the speed of light in vacuum, and n_{m} is the refractive index of the particle. The optical extinction force is only proportional to R^6 when the optical properties of the particle and medium are constant. The Equation S1 is the perturbative theory used to calculate the optical forces on the 100-nm nanoparticles in Figure 2.

The integrations over closed surfaces using Minkowski stress tensor can be distinct when the shape of the surface is different. Figure S3 shows the comparison of integration over the cube and sphere surfaces in water. The two integrations in a Gaussian beam matches well with each other when the gap is 15 nm. It shows slight mismatch in complex light fields, such as the light field in Figure S2. However, the shape and magnitude of the curves fairly matches. We also investigate the forces using two integration surfaces with different gaps in the *y*- and *x*-directions in Figures S4 and S5, respectively. It shows the best matching of two surfaces when the gap is 20 and 30 nm in the *y*-direction in Figure S2. And two methods match well with all gaps in the *x*-direction in Figure S4. Therefore, the gap from 20 to 30 nm is the best option for the simulation of optical forces using two methods. Especially, the integration over a cube surface is much easier to configure than a sphere surface.

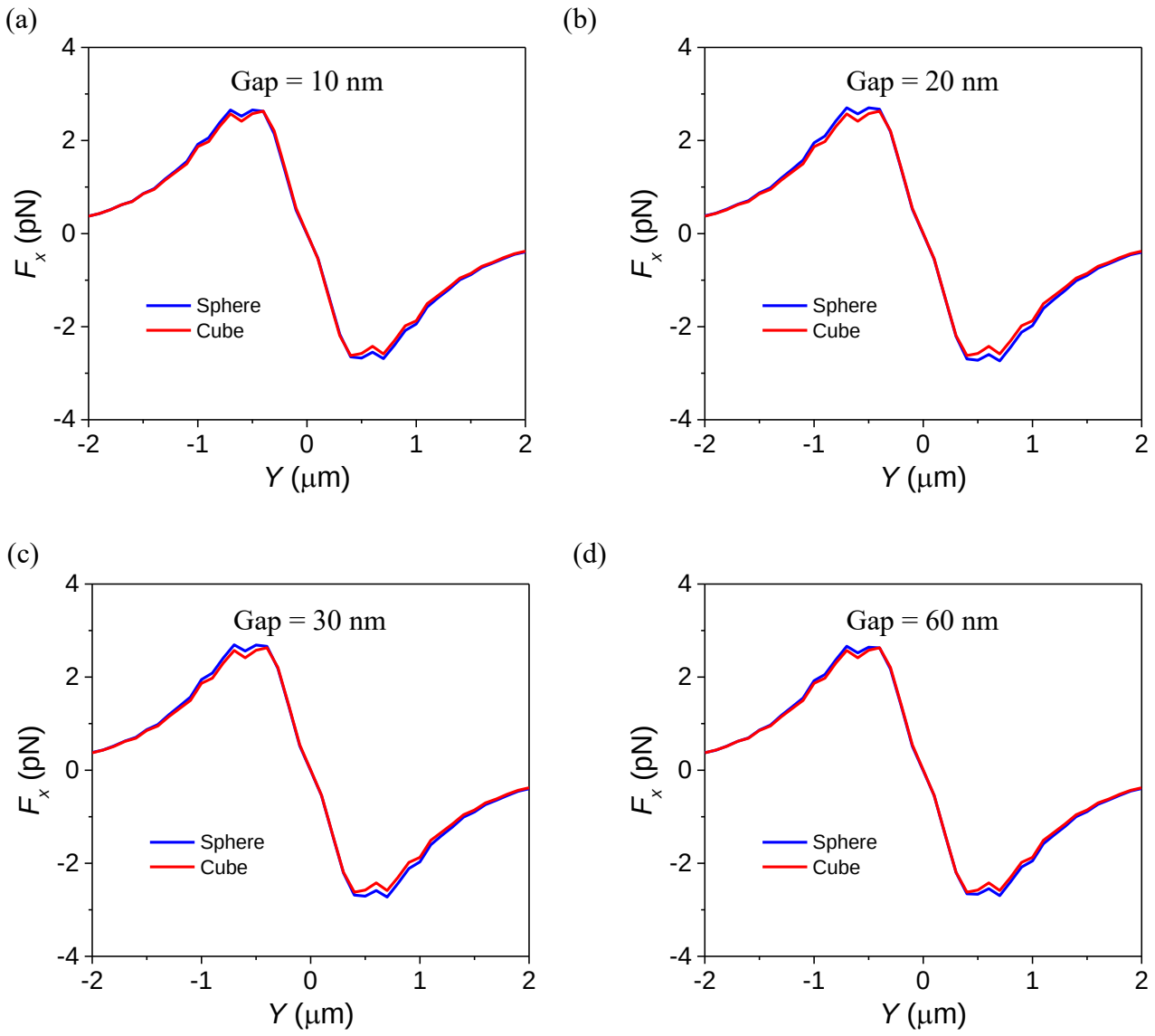

Figure S5. Comparison of the optical force in the *y*-direction in a Gaussian beam by changing the gaps. Calculated forces in the *y*-direction when the gaps between the integration surface and the particle are (a) 10 nm; (b) 20 nm; (c) 30 nm and (d) 60 nm. The maximum mesh in the simulation zone is 10 nm. Two methods match well with all gaps shown above.

We simulate the temperature increasement of a 1-μm bioparticle as shown in Figure S6. Since the oocyst is not absorbing, the temperature increasement is theoretically to be 0. To comprehend the temperature effect, we set the real and imaginary parts of the particle refractive index to be 1.5 and 10^{-5}, respectively. The 10^{-5} is a big value since the imaginary part of water is only 1.5×10^{-9}. The simulation

zone is a cube with a diameter of 1.5 μm. The laser and flow come from the left and right, respectively. The beam is polarized in the *y*-direction. It is shown in Figure S6d that the temperature becomes stable in 50 μs under the coordination of the laser illumination and flow dissipation. The increased temperature is eventually to be less than 1 ˚C even if the imaginary part of the refractive index is set to be 10^{-5} and the laser power is the 10^{10} W/m^2. Therefore, the heating effect is negligible in our optofluidic system.

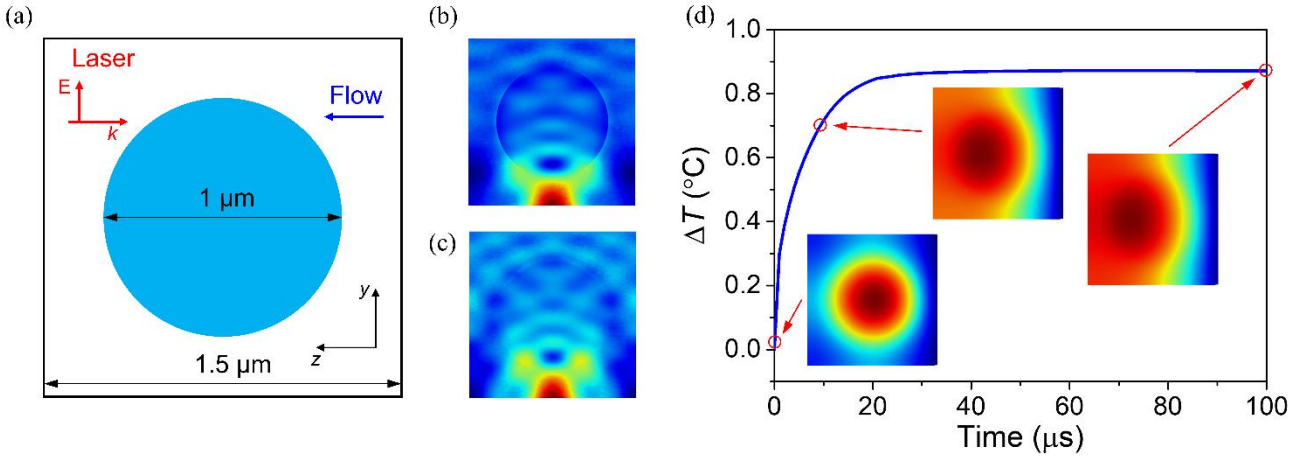

Figure S6. Simulation of the temperature of a 1-μm bioparticle. (a) Simulation model of the particle in an optofluidic system. The laser intensity is set to be 10^{10} W/m^2. And the flow velocity is 10 μm/s. Simulated electric fields in the (b) *x*-*z* and (c) *y*-*z* planes. (d) Increased temperature with time. Insets: temperature distributions at 1, 10 and 100 μs.

4. Optical hopping and pushing with high laser power

As shown in Figure S7, when the optical force is 3 time (900 mW) greater than that in Figure 3a, the optical extinction force in State 3 prevails over the drag force, which means that the particle would continue being pushed away from the second potential well by the optical force without generating a cyclic trajectory. In contrast, when the drag force is increased by twice (14 μm/s), the balance position becomes close to the position $x = 0$. The particle would be trapped stably inside the main hotspot and unable to hop to the adjacent one.

The Poynting vectors in the *x*-*y* plane when the particle is place at P2 and P3 are shown in Figure S8. It shows strong electric field on the right side of the 1-μm particle, which results in the enhanced forward scattering on the right of particle. This forward scattering in return generates a strong optical pulling force in the opposite direction of the Poynting vectors. On the contrary, Figure S8b shows a normal optical focusing effect which pushes the particle to the right side.

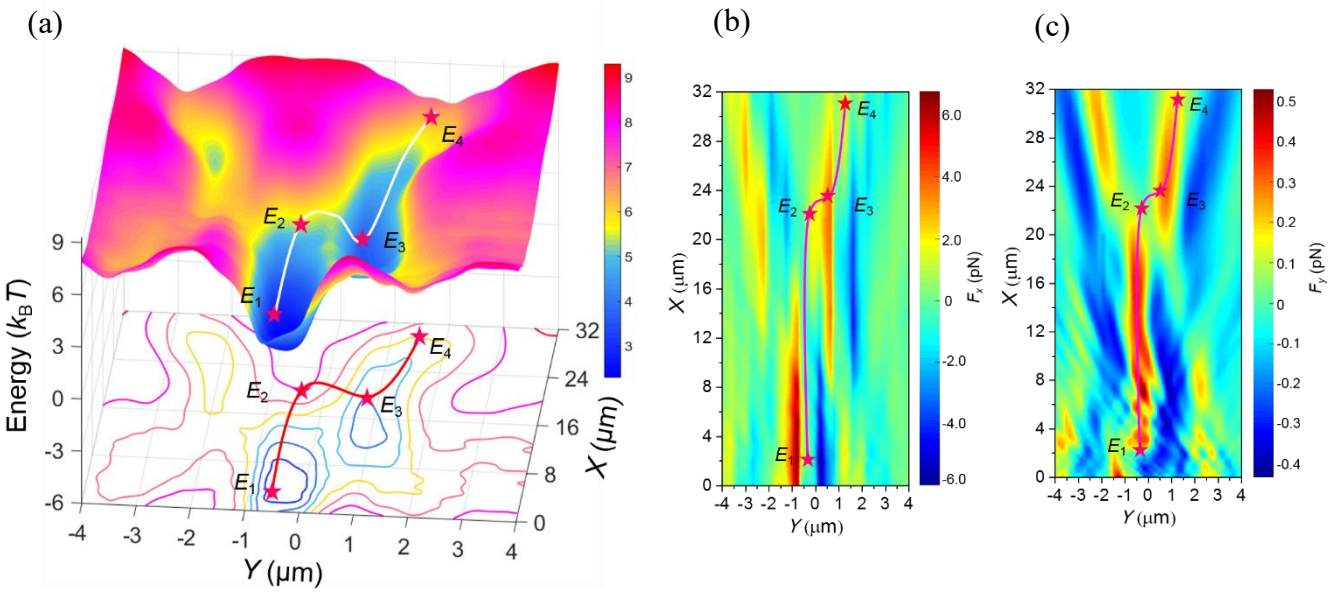

Figure S7. (a) Calculated potential energy when the laser is increased to 900 mW. The particle will further be pushed away by the optical forces when reaching State 3. Calculated overall forces (b) in the *x*-direction and (c) *y*-direction related to (a). The flow velocity remains 7 μm/s. To better show the potential energy landscapes and the contours, the landscape is upshifted by 8 k_BT.

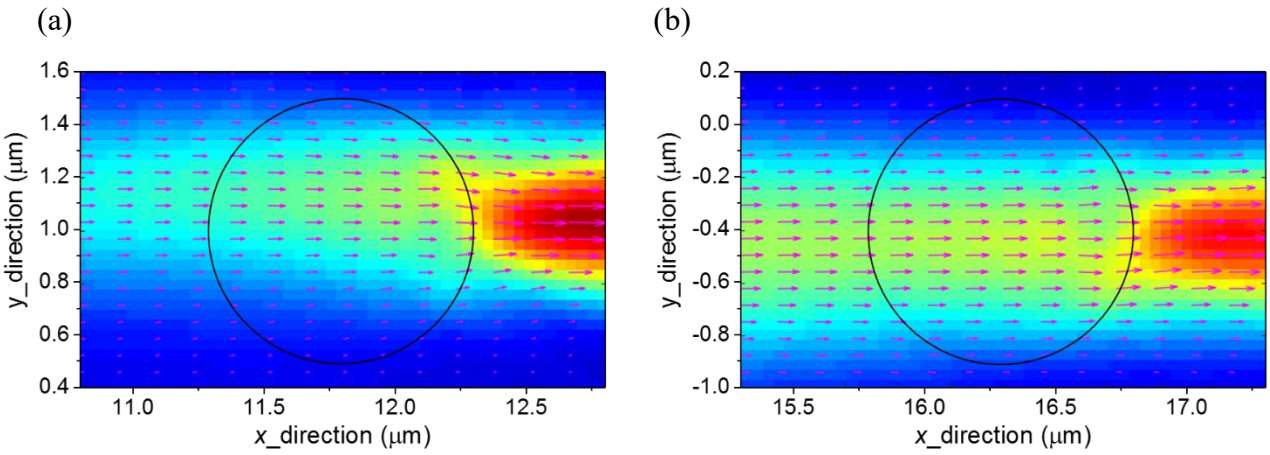

Figure S8. Poynting vectors in the *x*-*y* plane when the particle is placed at (a) P2 and (b) P3 in Figure 2. (a) Enhanced forward scattering Poynting vector indicates an optical pulling force. (b) Normal optical radiation pressure.

5. Velocity and work done by the optical and fluidic forces

The velocity of a single *Cryptosporidium* oocyst was shown in Figure S9. The oocyst got a positive velocity by the pushing of the optical scattering force. After hopping, the optical pulling force and fluidic drag force imposed a negative velocity to the oocyst. It had a positive force again after the hopping back to the State 1.

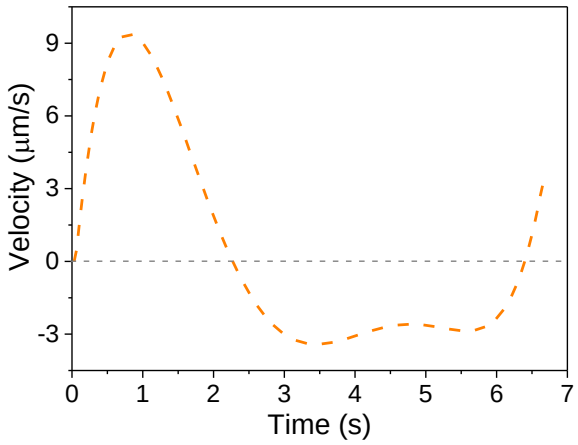

Figure S9. Velocity of a single *Cryptosporidium* oocyst in one cycle.

Since the two-dimensional force field is a non-conservative field with a non-conservative force F_{drag}, we calculate the total force by considering the particle is still in each position. Therefore, in each point, the total force can be defined as $F(x, y) = F_{opt}(x, y) + F_{drag} = F_{opt}(x, y) + 6\pi\eta a v$, where η and v are the viscosity and the velocity of the flow, respectively. To comprehend the energy in each point, we define the energy in the original point (point (0, -4) in Figure 2e) to be 0 as shown in Figure S10. We first integrate the forces along the *y*-direction to obtain the potential energy at the point (0, *y*) to be $U(0, y)$. Then the potential energy in point (*x*, *y*) can be expressed as $U(x,y) = U(0,y) + \int_0^x F(x,y)dx$. It is noted that this definition of potential energy may not be suitable for arbitrary two-dimensional force field, for example those fields with chaotic trajectories of particles. The method here illustrates the energy transfer clearly because the particle moves along a rectangle trajectory and the force in the *y*-direction is mainly contributed by the conservative optical gradient force.

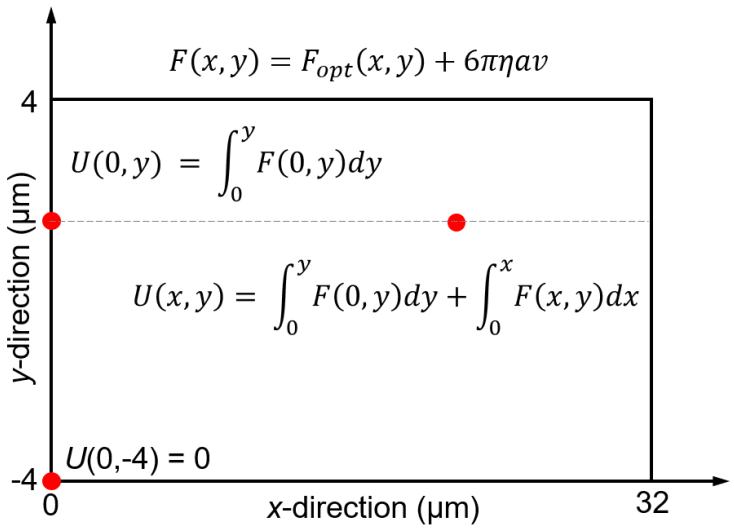

Figure S10. Illustration of force and potential energy calculation process in the two-dimensional light field.

6. Binding of oocyst and particles in the microchannel

Figure S11 shows the binding process of the *Cryptosporidium* oocyst and 1-um silica particles. The oocyst was moving in the microchannel when a pair of particles was approaching it at t = 0. They got contact with each other and bound together at t = 1.5 s. A third particle appeared at t = 2.8. It bound with the oocyst-particle complex at t = 3.7 s and started to move together.

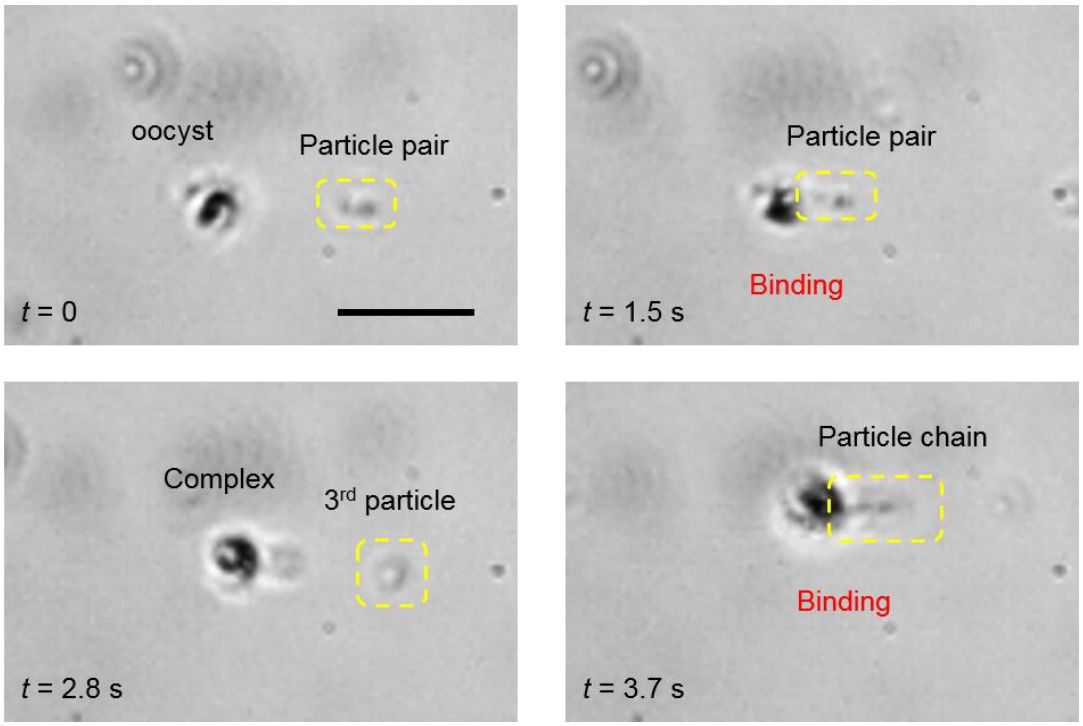

Figure S11. Binding procedure of the *Cryptosporidium* oocyst and 1 μm silica particles.